LAWRENCE
LIVERMORE
NATIONAL
LABORATORY

LLNL-TR-857394

VTO FY23 Annual Progress Report on 3D Printing of All-Solid-State Lithium Batteries

J. Ye, A. Orhan, M. Wood, E. Ramos

November 17, 2023

Disclaimer

This work performed under the auspices of the U.S. Department of Energy by Lawrence Livermore National Laboratory under Contract DE-AC52-07NA27344.

XIV Beyond Li-ion R&D: Solid-State Batteries

XIV.19 3D Printing of All-Solid-State Lithium Batteries (LLNL)

Jianchao Ye, Principal Investigator
Lawrence Livermore National Laboratory
7000 East Avenue
Livermore, CA, 94550
E-mail: ye3@llnl.gov

Simon Thompson, DOE Program Manager
U.S. Department of Energy
E-mail: simon.thompson@ee.doe.gov

Start Date: Jan 10, 2022 End Date: Jan 09, 2025
Project Funding (FY23): $375K DOE share: $375K Non-DOE share: $0

Project Introduction

All-solid-state lithium metal batteries (ASSLBs) have attracted attention due to their potential for mitigating safety issues and addressing energy density limitations of conventional lithium-ion batteries (LIBs). While solid-state electrolytes (SSEs) with room-temperature ionic conductivities greater than that of their liquid electrolyte counterparts have been discovered, integration of the different solid components of ASSLBs is not trivial. Taking garnet $Li_7La_3Zr_2O_{12}$ (LLZO) electrolyte as an example, problems for this SSE include brittleness, high temperature processing for densification, poor contact with electrodes, and lack of scalable manufacturing methods. These obstacles must be overcome before LLZO becomes commercially viable for ASSLB applications.

Realistic shape factors. Commercially available or lab-developed SSE discs must be thick (e.g., hundreds of micrometers to millimeters) to be mechanically robust enough to overcome their brittle nature, which unfortunately increases the cell impedance and accounts for the majority of overall cell weight and volume, leading to dramatically decreased power and energy densities. To increase energy density, membrane thickness has to be less than 100 µm and ideally < 20 µm. However, poor mechanical properties such as brittleness for pure oxide SSEs and low stiffness for polymer SSEs increase processing difficulty and promote defect-induced Li penetration. Ultrathin, flat and dense SSE membranes show high flexibility and thus can be stacked together with other electrode components for large scale battery assembly, though that the community suffers from a lack of cost-effective precision manufacturing methods for this purpose. Alternatively, composite polymer electrolytes with requisite active filler content and proper organization may increase mechanical flexibility while reducing manufacturing cost. However, these materials still suffer from conductivity, mechanical stiffness, and electrochemical stability issues which all must be addressed.

Electrode integration. Wetting of SSEs with metallic Li has been partially addressed by introducing lithiophilic interfaces, while the uniformity and cost of the artificial layer still need to be optimized. In addition, achieving good contact of SSEs with the cathode is still an issue. On one hand, co-sintering has been investigated to enhance the cathode contact via solid-state densification while kinetically limiting the chemical reactions. Our work on composite pellet co-sintering and slurry-based co-sintering has shown reasonable thermal stability between Ta-doped LLZO (LLZTO) and NMC 622 at 900 °C. However, issues like mechanical robustness due to relatively high porosity still need to be solved. In addition, carbon additives need to be introduced to provide electronically conductive pathways for these relatively thick electrodes. On the other hand, cathode slurries with polymer binders have often been spread on the sintered LLZO films for cell assembly. The use of polymer binder

may sacrifice the operational temperature and lower electrochemical stability. A small amount of liquid electrolyte/solvent is usually applied to enhance the contact, which negates some of the safety benefits of all-solid-state batteries. A highly conductive solid catholyte with stable and good contact with cathode will be necessary to facilitate Li^+ transport.

Scaling up approach. Unlike liquid electrolyte-based LIBs for which roll-to-roll (R2R) methods have been developed for large scale manufacturing, scaling up of SSBs is likely different. Although soft and glassy sulfide-based SSBs are promising candidates for R2R manufacturing, their interfacial stability with electrodes must be resolved. For garnet LLZO-based SSBs, composite polymer electrolytes may be most ready for meaningful demonstrations of scaling up, though their Li+ conductivity still needs improvement. Pure ceramic-based SSBs will likely require one-step formation to avoid repeated deformation induced cracking.

Cycling stability. Even with successful manufacturing of an ASSLB, poor cycling stability can still limit performance. Several failure mechanisms must be overcome include (but are not limited to): 1) void formation at the Li anode side during Li stripping; 2) Li dendrite nucleation and penetration; and 3) cracking/delamination on the cathode side. Effective characterization methods that help shed light on the failure mechanisms will be critical for designing better materials and manufacturing approaches that stabilize the long-term cycling performance.

Objectives

Specific Objective 1: Down select 3D printing and post processing approaches for SSE/cathode integration
Specific Objective 2: Understand battery failure mechanisms via ex situ and in situ characterization

Approach

The technical approaches include advanced manufacturing based on 3D printing and related techniques, ex situ/in situ characterizations, and battery testing. In addition to experimental efforts, the team will work closely with the computational partner (PI: Brandon Wood) to better understand battery failure mechanisms and design new battery architectures and chemistries for performance improvement. 3D printing approaches will be optimized and down selected to fabricate 3D interfaces for battery performance evaluation. Three approaches including sintering-free, hybrid, and co-sintering will be studied. Ex situ and in situ characterizations will be developed to understand battery failure mechanisms. Routine electrochemical and basic characterizations will be used for troubleshooting. In situ Raman and KPFM techniques will be conducted to analyze the electro-chemo-mechanical evolution of printed ASSLBs.

Results

UV-curable PEGDA/PEGMEA/PEO-LLZTO composite polymer electrolytes

The team used UV curable PEGDA/PEGMEA/PEO-LLZTO as a model system to study the relationship of ionic conductivity and Young's modulus with LLZTO particle content, and explore different strategies to integrate the resulted CPE with LFP cathode and Li anode for cell performance test.

The CPE membranes were prepared by tape casting of homogeneous slurries composed of PEGDA, PEGMEA, PEO, LiTFSI, LLZTO, and other additives. After UV curing and 80°C vacuum drying overnight, freestanding films were formed (Figure XIV.19.1a). Modulus of the CPE with LLZTO content up to 10wt% was measured by AFM nanoindentation in Ar glovebox. Figure XIV.19.1b shows the modulus decreases from 6 MPa without LLZTO to 1 MPa at 7 wt%. Correspondingly, Li symmetric cells show the ionic conductivity of CPE increases from 2×10^{-5} S/cm to 2×10^{-4} S/cm (Figure XIV.19.1b). Strong trade-off between modulus and ionic conductivity can be explained by the reduced crosslinking degree and amorphization. The CPE with 7wt% LLZTO (CPE7) can be cycled in Li symmetric cells (Figure XIV.19.1c) at room temperature, although the overpotential at 0.1 mA/cm^2 increases gradually from 0.14V up to 1V after 76 cycles.

FEC has been found to improve the SEI quality in liquid electrolyte based LIBs and was recently found to be beneficial for polymer electrolytes [1]. Here, the team added 1wt% of FEC in the CPE and studied its effects in the mechanical, electrochemical properties and cell performance. AFM nanoindentation reveals the improvement of Young's modulus, from 1 MPa to 5 MPa, making the casted film easy to peel off from the glass slide substrate. This improved mechanical property is beneficial to mitigating dendrite penetration issue and reduce the chance of short circuit during cell assembly and testing. With the increase of mechanical properties, trade-off is observed with ionic conductivity reduced to 2~5 x 10^{-5} S/cm at room temperature. However, heating it up to 60 °C gives a 10 times higher conductivity (4 x 10^{-4} S/cm). Li symmetric cells show Li plating/stripping overpotentials gradually increase from 24 mV to 50 mV at 0.1 mA/cm^2 after 33 cycles. Lower the temperature to 45 °C leads to an increase of overpotential to 140 mV and gradually to 270 mV after 35 cycles.

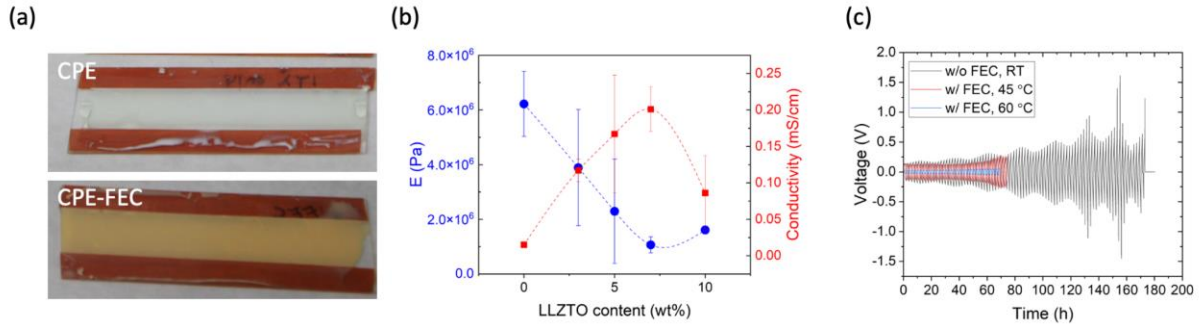

Figure XIV.19.1 Composite polymer electrolytes. (a) Tape casted CPE films with (bottom) and without (top) FEC additive. (b) Young's modulus (E) and ionic conductivity as functions of LLZTO weight percentage in PEGDA/PEGMEA/PEO-LiTFSI polymer electrolytes. (c) The Li plating/stripping cycling stability test with 0.1 mA/cm2 current density and 1h plating/stripping period.

The team assembled solid state cells using the developed CPEs, with LFP as cathode and Li as anode. Tape casted LFP films were employed before diving into 3D printed counterparts. The CPE were either infilled into as casted or calendered LFP films, or directly attached to calendered LFP films for coin cell assembly (Figure XIV.19.2). The comparison reveals the importance of forming and maintaining intimate contact for facile Li^+ and electron transport.

For example, as shown in Figure XIV.19.2a, infilling CPE into uncalendared LFP film could break down the connections between LFP particles, leading to the loss of materials and therefore lower capacity. This can be a serious issue when the solvents in the CPE precursors attack the PVDF binder. To improve physical contact in the cathode, the as tape casted cathode was calendered using a hot roller press. CPE was infilled into calendered cathodes to compare with the as-casted cathode (Figure XIV.19.2c). Free-standing CPE film was stacked onto calendered cathode to make another cell without catholyte infilling for performance comparison (Figure XIV.19.2b). Generally calendered cells show higher capacity than as casted cell, suggesting some active materials in the as casted cathode are not in good contact with the current collector or adjacent carbon black particles after CPE infilling. Upon cycling, volume change may further weaken the particle-particle contact and therefore leads to continuous material loss. Using freestanding CPE in the calendered cell with LFP mass loading of 5 mg/cm^2, the team demonstrated a cell with high initial capacity of 145 mAh/g at RT, but the value dropped quickly to 110 mAh/g in the third cycle. It is likely that insufficient ion transport pathway in this case led to fast capacity decay. By infilling the CPE into calendered cathode to provide ion transport medium, the capacity reaches 150 mAh/g, and

maintains that value in the following two cycles. Compared with as casted electrodes, the IR drop decreases from 168 mV to 48 mV after calendering. EIS also shows the reduction of interfacial resistance by adopting infilled calendered cathode, suggesting the gain of electrochemical surface area. Calendering strengthens the bonding between active materials and therefore can maintain good electrical contact during processes including CPE infilling, vacuum drying, and UV cure. However, due to the weak mechanical properties of the CPE7 electrolyte, Li dendrite penetration leads to micro-shorts that cause the voltage noise in the charging period (Figure XIV.19.2c).

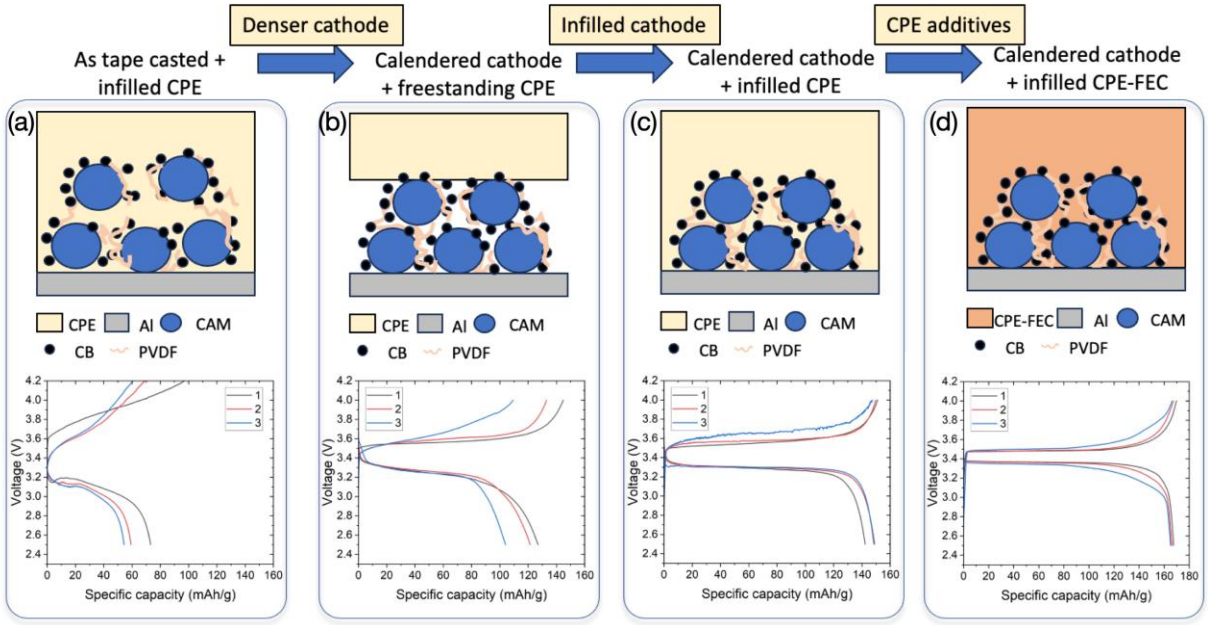

Figure XIV.19.2. Four LFP-Li cells with different integration methods showing the improvement of charge/discharge capacity at C/10 rate.

By adding 1 wt% FEC in process of CPE7F, The LFP-CPE7F-Li Cell (as casted LFP) shows stable cycling with capacity of 115 mAh/g at C/20, and ~ 90 mAh/g at C/10 at 45 °C. Stable charging/discharging with no overpotential increase or microshorts was observed in the current 13 cycles at slow rates. Further increasing the temperature to 60 °C led to a capacity of 135 mAh/g at C/20. EIS shows that both the bulk and interfacial impedance decreased 10 times with increasing temperature to 45 °C, which is in contrast to the CPE without FEC that showed interfacial resistance decrease of only 22 % with increase temperature to 60 °C. This strongly indicates that FEC stabilizes the SEI layer with metallic Li anode. Using a calendered LFP for the CEP7F cell (Figure XIV.19.2d) leads to further enhancement of the cell performance with close to 170 mAh/g specific capacity at C/10 rate at 60 °C and smooth voltage profiles.

Co-sintering of LLZTO/LiCoO2.

Co-sintering the cathode and electrolyte together has the potential to improve interfacial contact. However, the team observed that the $Li_{6.4}La_3Zr_{1.4}T_{0.6}O_{12}$ (LLZTO) solid electrolyte changed color from white to green when it was co-sintered with an $LiCoO_2$ (LCO) cathode using conventional furnace sintering (Figure XIV.19.3a). The team conducted experiments to determine the cause of this color change and its effect on the structure, mechanical properties, and conductivity of the LLZTO.

Element analysis was conducted using inductively coupled plasma-optical emission spectroscopy (ICP-OES) and instrumental gas analysis (IGA for oxygen), on the LLZTO pellet after co-sintering with a layer of LiCoO2. The table in Figure XIV.19.3b confirm the presence of a very small amount of cobalt (0.11 wt%) in the LLZTO pellet after co-sintering, resulting in a composition of $Li_{6.3}La_3Ta_{0.6}Zr_{1.4}Co_{0.02}O_{11.3}$. These results suggest that in addition to cobalt entering the LLZTO structure, some lithium and oxygen may have been lost during co-sintering. These Co-doped LLZTO pellets were also analyzed by XRD to identify any structural changes that may have taken place as a result of the Co diffusion into the LLZTO lattice. The XRD results are shown in Figure XIV.19.3c. Overall, the small level of Co-doping does not seem to have much of an effect on the overall structure of the LLZTO.

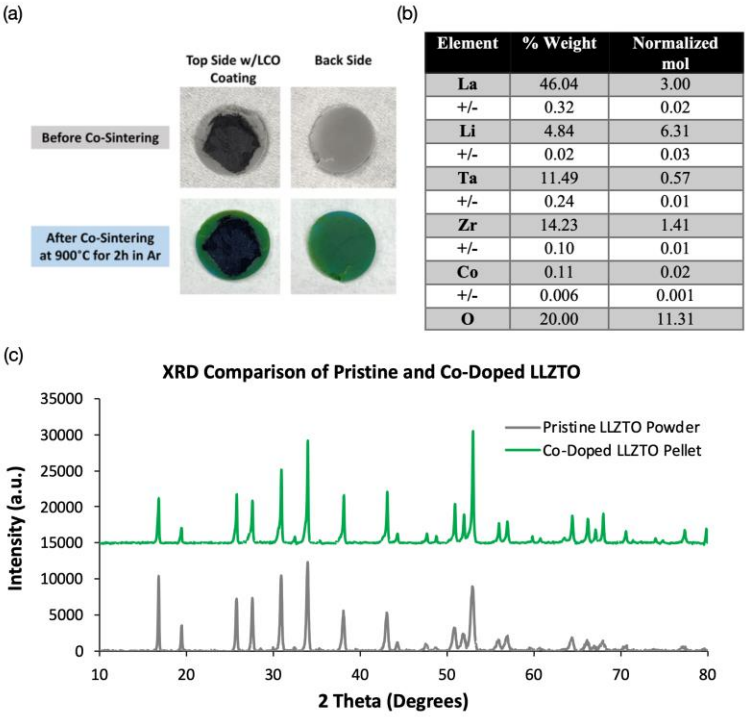

Element	% Weight	Normalized mol
La	46.04	3.00
+/-	0.32	0.02
Li	4.84	6.31
+/-	0.02	0.03
Ta	11.49	0.57
+/-	0.24	0.01
Zr	14.23	1.41
+/-	0.10	0.01
Co	0.11	0.02
+/-	0.006	0.001
O	20.00	11.31

Figure XIV.19.3 (a) Pictures of sintered LLZTO pellets coated with a layer of LCO before and after co-sintering at 900 °C for 2h in Ar. (b) ICP-OES (all elements except for oxygen) and IGA analysis (oxygen) of LLZTO pellets after co-sintering with LCO. The LCO layer was removed before analysis. (c) XRD comparison of pristine LLZTO powder and Co-doped LLZTO pellets (prepared by removing the LCO layer after co-sintering with LCO at 900 °C for 2h in Ar).

Nanoindentation tests were performed on the Co-doped LLZTO pellets to determine the effect of Co diffusion on the mechanical properties. Nanoindentation tests reveal a decrease of Young's modulus and hardness with Co diffusion. Pristine LLZTO pellets show a Young's modulus of 156.5 ± 5.1 GPa and hardness of 8.81 ± 0.75 GPa. With Co diffusion, the Young's modulus decreases to 139.9 ± 4.3 GPa and the hardness to 7.31 ± 0.41 GPa. Nanoindentation load-displacement curves (Figure XIV.19.4a) also show viscoplastic creep behavior changes with Co diffusion. The increased creep displacement for a given load holding time (10s) suggests microstructural variation that introduces an additional deformation mechanism after Co diffusion. It is hypothesized that Co accumulation in the LLZTO grain and grain boundaries may lead to a higher degree of amorphization, weaken the grain boundaries and cause grain sliding/rotation under load, but detailed atomic scale characterization may be necessary to reveal the underlying physics.

Electrochemical impedance spectroscopy (EIS) was used to determine the effect of Co-doping on the ionic and electronic conductivities of LLZTO. Gold paste was applied to the surfaces of the LLZTO pellets to serve as ion-blocking electrodes. EIS plots (Figure XIV.19.4b) were fit by a simple (Q1+Q2/R2) equivalent circuit model to obtain the solid state electrolyte resistance R2. The measured ionic conductivity of pristine LLZTO at RT was 0.35 mS/cm. After co-sintering with LCO, the conductivity decreased to 0.21 mS/cm. This result implies that co-sintering induced Co diffusion may adversely impact the LLZTO separator. The electronic conductivity was measured by applying a DC voltage bias (0.3V) for 3 hours (Figure XIV.19.4c). It was found that with Co doping, the electronic conductivity also decreased from 2.5 nS/cm to 1.9 nS/cm. The decrease of electronic conductivity is beneficial for LLZTO separator but may reduce electron transport in the LLZTO/LCO composite cathode.

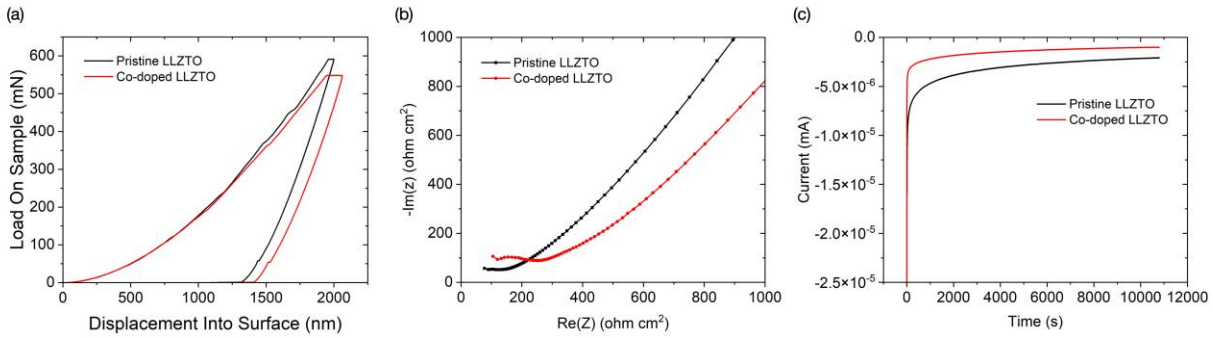

Figure XIV.19.4 (a) EIS plots and (b) DC polarization curves of pristine and Co-doped LLZTO pellets with Au as ion blocking electrodes.

Conclusions

In FY23, > 10^{-4} S/cm ionic conductivity at room temperature was achieved in UV-curable PEGDA/PEGMEA/PEO-LLZTO composite polymer electrolytes. The ionic conductivity reaches a peak value 2 x 10^{-4} S/cm with 7wt% LLZTO additive. In the meantime, the modulus is down to a valley value of 1 MPa. The Li symmetric cells show a gradual increase of over potential, suggesting the accumulation of SEI or mossy lithium. The low modulus of the CPE also adds challenge to assemble cells with 3D printed electrodes due to the local high pressure induced short circuit. The addition of 1wt% FEC significantly increases modulus (5x) and interfacial stability. With further strenghtening of electrode films by calendering, the cell performance was dramatically improved. In a parallel study, the team found that co-sintering LLZTO/LCO using conventional furnace sintering leads to a decrease in the ionic conductivity, electronic conductivity, modulus, and hardness of LLZTO. The findings provide important information in the failure mechanisms of solid-state batteries with co-sintered cathode.

Key Publications

Talks:

1. UC Davis chemical engineering seminar, Davis, California (January 12, 2023): “Additive Manufacturing for Energy Applications”. Invited.
2. 2nd Edition of TechBlick's Next Generation &Beyond Li-Ion Battery Materials Conference, virtual (February 15, 2023): “Laser Sintering of Solid-State Electrolytes”. Invited.

3. 40th International Battery Seminar & Exhibit, Orlando, Florida (March 20-23, 2023): "Additive Manufacturing for Battery Applications". Invited.
4. ACS Spring 2023, Indianapolis, Indiana (March 26-30, 2023): "Laser Sintering of Solid-State Electrolytes". Invited.
5. Workshop on Electrochemical Interfaces: Advancing the integration between multiscale modeling and multimodal characterization. Livermore, CA. (September 28-29, 2023): "Additive Manufacturing Tools to Facilitate Battery Research and Manufacturing".
6. FY23 Solid State Engineering Lab Review Meeting. Berkeley, California (August 30-31, 2023): "Three-Dimensional Printing of All-Solid-State Lithium Batteries".

References

1. Lin, R., et al., *Characterization of the structure and chemistry of the solid–electrolyte interface by cryo-EM leads to high-performance solid-state Li-metal batteries.* Nature Nanotechnology, 2022. 17(7): p. 768-776.

Acknowledgements

LLNL Team members who have contributed to the project in FY23 include Asya Orhan, Erika Ramos, Marissa Wood, Yuliang Zhang, and Sijia Huang. We also acknowledge Bo Wang, Tae Wook Heo, and Brandon Wood from LLNL simulation group, as well as Sangil Kim from University of Illinois at Chicago, Huolin Xin from University of California at Irvine for discussions and collaborations.